Rare Metal Materials and Engineering
Volume 46, Issue 9, September 2017
Online English edition of the Chinese language journal

Available online at www.sciencedirect.com
ScienceDirect

Cite this article as: Rare Metal Materials and Engineering, 2017, 46(9): 2437-2444.

ARTICLE

Corrosion Behavior of Friction Stir Welded Al-Mg-(Zn) Alloys

Hou Longgang[1], Yu Jiajia[1], Zhang Di[1], Zhuang Linzhong[1,2], Zhou Li[3], Zhang Jishan[1]

[1] *State Key Laboratory for Advanced Metals and Materials, University of Science and Technology Beijing, Beijing 100083, China;* [2] *TaTa Steel, 1970 CA IJmuiden, The Netherlands;* [3] *Shandong Provincial Key Laboratory of Special Welding, Harbin Institute of Technology at Weihai, Weihai 264209, China*

Abstract: The corrosion behavior of friction stir welded Zn-modified Al-Mg alloys was investigated as well as the effects of pre-weld temper conditions on the corrosion behavior of the friction stir welded alloys. Results indicate that both maximum corrosion depth and dominating corrosion mode in different weld regions after post welding heat treatment show obvious variations with an increase in the Zn content. With Zn additions the dominating corrosion mode changes from intergranular corrosion to pitting corrosion, and the severe galvanic corrosion tendency obviously occurs in the precipitation hardened alloys compared to that of the strain hardened alloy. This would be greatly related to the formation of discontinuously distributed grain boundary precipitates as well as abundant intragranular precipitates (mainly T-AlZnMgCu phase) in the precipitation hardened Al-Mg-Zn alloys while it is associated with the continuously distributed β-AlMg phase along grain boundary in the Zn-free Al-Mg alloys.

Key words: Al alloy; friction stir welding; intergranular corrosion; precipitate; microstructure

Friction stir welding (FSW), as a solid phase joining technique by locally introducing frictional heats and plastic flow via rotating the welding tools, can be used to join high strength Al alloys, which is considered non-weldable with conventional fusion welding technique. FSW process generates four distinct microstructural zones: unaffected material or base metal (BM), heat affected zone (HAZ), thermal mechanically affected zone (TMAZ) and nugget zone [1,2]. For the corrosion potential differences among these four zones, the galvanic cells between them can appear and inevitably cause corrosion. Different zones are expected to exhibit different corrosion depths and modes [3].

The corrosion behavior of the FSWed Al alloys has been widely studied and the corrosion resistance of the non heat-treatable Al alloy cannot be altered significantly by welding heats. For FSWed 5456 Al alloy, the corrosion of the nugget zone was slightly higher than that of BM[4,5]. However, in the precipitation hardened Al alloys, the corrosion resistance after welding was much complicated and affected by alloy compositions and welding processes. For 2050 and 7108 Al alloys, the TMAZ and nugget zone were much easier to be corroded with BM and HAZ being protected[6,7]. For 2024-T351 Al alloy, the corrosion was easier to occur at higher rotational speed in HAZ while at lower rotational speed in the nugget region[8]. Also, a higher cooling rate after FSW resulted in a higher corrosion resistance [9]. Not only increasing the hardness and mechanical properties by reprecipitation[10-12], the post-welding heat treatment (PWHT) was another important factor affecting the corrosion resistance of the precipitation hardened Al alloys. Previous researches demonstrated that PWHT could dramatically decrease the intergranular corrosion depth after FSW[13-15], in which the dominating corrosion mode was changed from intergranular to pitting corrosion after PWHT[16].

Traditional Al-Mg alloys are extensively used in marine and armor vehicle transportations, due to their good corrosion resistance, weldability, formability and reasonable strength. These alloys are typically strengthened and hardened by solid solution strengthening and strain hardening, and designated by H321 and H116 tempers for shipbuilding industry, and by

Received date: September 02, 2016
Foundation item: National Natural Science Foundation of China (51301017, 51571013); Beijing Laboratory of Metallic Materials and Processing for Modern Transportation, China; State Key Lab of Advanced Metals and Materials, China (2014Z-09)
Corresponding author: Zhang Di, Ph. D., Associate Professor, State Key Laboratory for Advanced Metals and Materials, University of Science and Technology Beijing, Beijing 100083, P. R. China, Tel: 0086-10-82375844, E-mail: zhangdi@skl.ustb.edu.cn

H131 and H136 tempers for armor vehicle industry. By adding some Zn element, the Zn-containing precipitates will act as the main precipitation-strengthening phase inside the grains for the newly developed Al alloy that will simultaneously possess strain hardening, solid solution strengthening and precipitation hardening via optimizing the ageing and precipitation processes, thus greatly increasing the strength[17,18]. The present work aims to investigate how the corrosion behavior can be related to Zn additions in the FSWed Al-Mg alloys. The microstructures as well as the morphology of the grain boundary precipitates (GBPs), the precipitate free zone (PFZ) and the precipitate distribution in the grains were observed, and the corresponding relationship among corrosion behavior, microstructure, and Zn content will be established.

1 Experiment

1.1 Materials and FSW

Three Al-Mg-(Zn) alloys were designed presently: alloy 1 (Al-6.0Mg-0Zn, wt%), alloy 2 (Al-6.3Mg-1.0Zn, wt%) and alloy 3 (Al-6.2Mg-2.0Zn, wt%), and they also contained some other elements: 0.8Mn, 0.07Ti, 0.15Si, 0.15Zr, 0.15Cu, 0.2Fe, and 0.03Cr (wt%). The ingots were homogenized and hot rolled to 6 mm, then cold rolled and full recrystallized with subsequent cold rolling to 2.5 mm. They were divided into two groups: (1) A: stabilized at 250 ℃ for 1 h (H321 temper (strain hardened alloy)); (2) B: solution treated at 530 ℃ for 10 min, water quenched and subsequently aged at 90 ℃ for 24 h and 180 ℃ for 7 h (T6 temper (precipitation hardened alloy)). All the samples were finally stretched for 1%.

The dimension of the plates for friction stir welding was 300 mm×53 mm×2.5 mm. Two plates were butted joined together by FSW with a rotational speed of 850 r/min and a transverse speed of 150 mm/min. The welding direction was parallel to the rolling (longitudinal) direction of the plates. A friction stir tool was composed of a truncated cone-shaped pin (diameter: 2.35 mm) and a shoulder (diameter: 7.5 mm). After welding, all specimens were subjected to a PWHT at 100 ℃ for 7 d.

1.2 Corrosion and mechanical testing

Before corrosion tests, the samples cut from the welding plate were degreased in acetone, alkaline etched in 7.5 wt% NaOH at 55~60 ℃ for 5 min and then washed with distilled water. The samples were subsequently immersed in an acidified salt solution (30 g NaCl and 10 ml concentrated HCl per litre) at 35 ℃ for 1 h and 6 h, respectively, washed with distilled water and ethanol, and then dried. The long transverse-short transverse (LT-ST) cross sections of the corroded alloys were polished and observed by optical microscopy. The corrosion susceptibility was evaluated by measuring the maximum corrosion depth. Vickers hardness was measured using 0.2 kg loads on the LT-ST surface.

1.3 Microstructure observation

Specimens in different welding regions after FSW were prepared by mechanical polishing and etched in 40% phosphoric acid at 50 ℃ for 3 min and observed by optical microscopy. Transmission electron microscope (TEM) studies were carried out on the BM and nugget zone of all PWHT specimens using Philips CM-20 FEG to reveal the distribution and morphologies of the precipitates both along the grain boundary and in the matrix. TEM samples were firstly mechanical-thinned and then thinned by twin-jet polishing technique in a solution (30 vol% nitric acid and 70 vol% methanol) at –20 ℃ with an applied current of 60 mA.

Statistical analysis of the percentage of grain boundary covered by precipitates were quantified for approximately 20 grain boundaries, while the width of PFZs were quantified for more than 100 positions from more than 10 TEM images for each condition. The number density and average size of the precipitates during different aging treatments were quantified for approximately 5 TEM images.

The FSWed alloys were electrochemically polished with perchloric acid and ethanol solution, anodized with Barker's solution (25 mL HBF_4 + 475 mL H_2O), and then observed using a polarized-light microscope. The average grain sizes in different welding regions were measured using a mean linear intercept method.

1.4 Electrochemical testing

Electrochemical experiments were carried out on electrochemical workstation using the three electrode system. A large platinum sheet was used as the counter electrode, and a supersaturated calomel electrode was served as the reference electrode. FSW welds in different regions with a dimension of 5 mm×5 mm×thickness were used as the working electrode. The specimens for electrochemical experiments were immersed into 450 mL 3.5 wt% NaCl solution at 25 ℃. The polarization experiments were performed with a scan rate 1 mV/s. The corrosion current densities/corrosion potentials was the average values of three parallel tests.

2 Results and Discussion

2.1 Hardness profile and microstructure of the FSW joints

The hardness distribution across the FSW joints for all three alloys demonstrates typical "W" shaped hardness distribution (Fig.1), similar to many FSW joints of the precipitation hardened Al alloys. The hardness in different weld regions is increased with an increase of the Zn content for both strain hardened and precipitation hardened Al alloys. And the hardness of the nugget zone may be slightly larger than the BM for the precipitation hardened Zn-free Al alloy (Fig.1b), due to hot work hardening and grain refinement. For Zn-containing Al alloys, the relatively higher hardness in the nugget zone is due mainly to the homogeneous precipitation of Zn-containing phases. For the strain hardening Al alloys, the severe deformation caused by FSW processing mainly contributes to the enhanced hardness across the FSW joints. The lowest hardness appears at the TMAZ/HAZ boundary for both precipita-

tion hardened and strain hardened Al-Mg-(Zn) alloys.

For the strain hardening alloys, Fig.2 shows that continuous distribution of GBPs in different welding regions is observed in the Zn-free alloy. For Alloy 2, the GBPs are discontinuously distributed along the grain boundary in the BM and HAZ, while continuously distributed along the grain boundary in the TMAZ and nugget zone. For Alloy 3, the GBPs are discontinuously decorated along the grain boundary in different welding regions. For the precipitation hardened temper, Fig.3 shows the microstructures in different welding regions for all the alloys are decorated by continuous GBPs. The grain size in the nugget zone is so small that the GBPs distribution should be further checked under higher magnifications.

2.2 Corrosion behavior of the FSW joints and polarization curves

As shown in Table 1, the maximum corrosion depths in the BM and HAZ are higher than those in the TMAZ and nugget zone for Alloy 1. However, for Zn-containing Al alloys, the maximum corrosion depths in the BM and HAZ are much lower than those in the TMAZ and nugget zone. For the precipitation hardened Al alloys, it can be seen that the maximum corrosion depths in the BM and HAZ are much higher than those in the TMAZ and nugget zone. For the Zn-containing Al alloys, the aging treatment enhances the corrosion depth of the BM and HAZ regions but still reduces the corrosion depth of the TMAZ and nugget zone. Thus, the microstructural evolution induced by aging Zn-containing Al alloys has a great influence

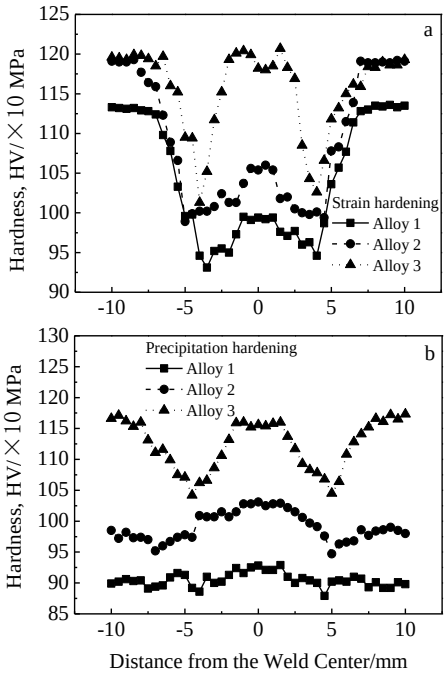

Fig.1 Micro-hardness profiles across friction stir weld joints of all three alloys in the strain hardening temper (a) and precipitation hardening temper (b)

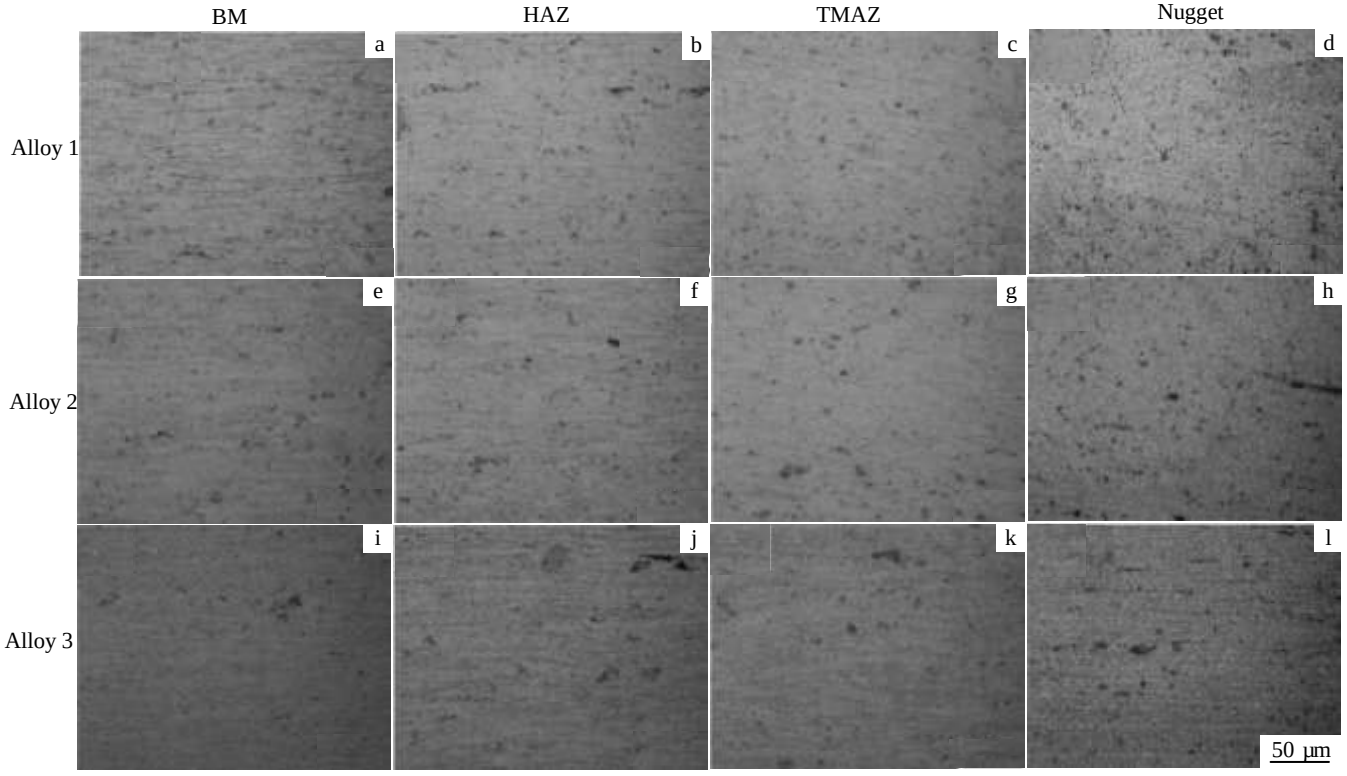

Fig.2 Optical microstructures of the strain hardened alloy 1 (a~d), 2 (e~h), and 3 (i~l) in different weld regions: (a, e, i) BM, (b, f, j) HAZ, (c, g, k) TMAZ, and (d, h, l) nugget zone

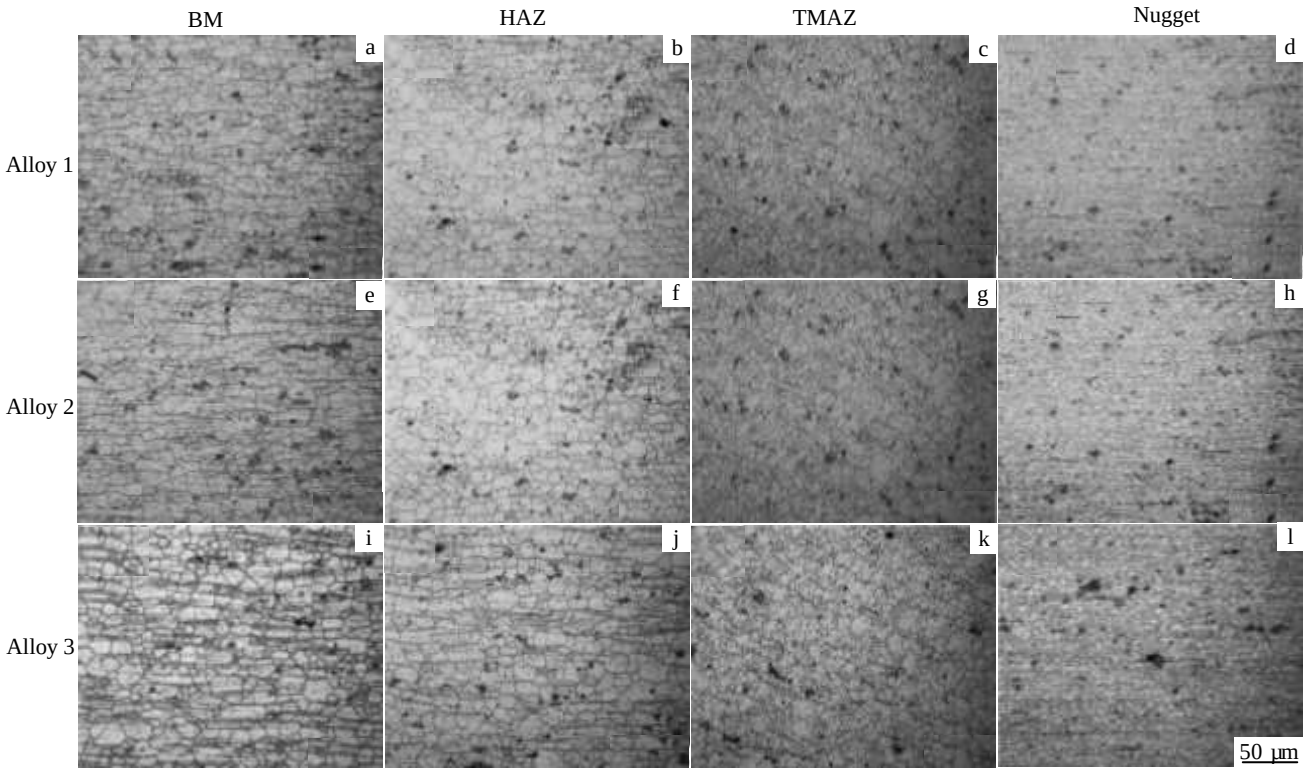

Fig.3 Optical microstructure of the precipitation hardened alloy 1 (a~d), 2 (e~h) and 3 (i~l) in different weld regions: (a, e, i) BM, (b, f, j) HAZ, (c, g, k) TMAZ, and (d, h, l) nugget zone

Table 1 Maximum corrosion depths (1 h/6 h) in different welding regions of all three alloys in the strain hardening and precipitation hardening tempers (μm)

Region		BM	HAZ	TMAZ	Nugget
Strain hardened alloy	1	15/56	15/33	0/24	0/10
	2	8/25	10/25	15/52	17/44
	3	7/10	4/9	146/338	33/111
Precipitation hardened alloy	1	62/169	56/93	4/6	0/0
	2	121/143	152/329	34/74	17/53
	3	158/452	111/243	58/117	56/83

on their corrosion behaviors, especially to the BM and HAZ zones. Typical microstructures after corrosion in Fig.4 shows the current corrosion is dominated by intergranular corrosion (Fig.4a, 4c) and pitting corrosion (Fig.4b). The dominating corrosion modes in different welding regions after corrosion testing are shown in Table 2. For the strain hardened Al alloys, it shows that all welding regions for Alloy 1, and the TMAZ and nugget zone for Alloy 2 are controlled by intergranular corrosion (IGC), while the BM and HAZ for Alloy 2 and all welding regions for Alloy 3 are dominated by pitting corrosion. The dominating corrosion mode for the precipitation hardened

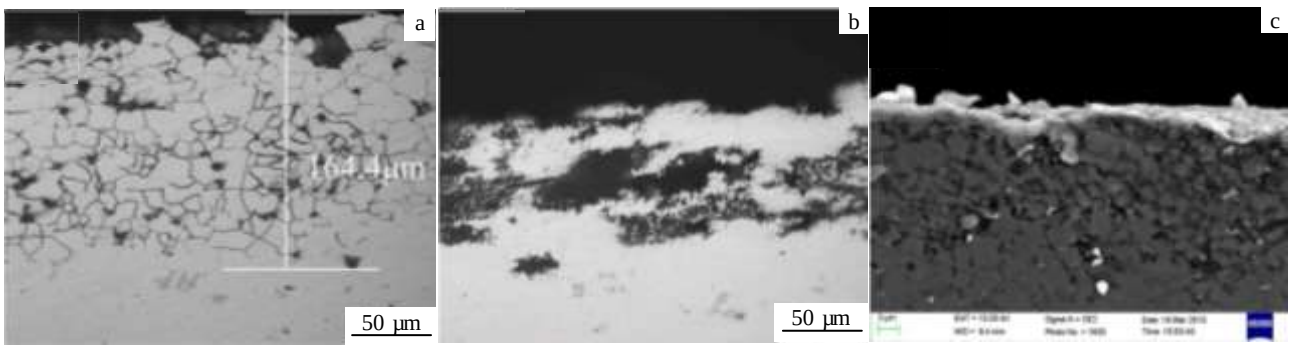

Fig.4 Typical microstructures of intergranular (a, c) and pitting corrosions (b)

Table 2 Dominating corrosion mode for all three alloys in the strain hardening and precipitation hardening tempers

Region		BM	HAZ	TMAZ	Nugget
Strain hardened alloy	1	IGC	IGC	IGC	IGC
	2	Pitting	Pitting	IGC	IGC
	3	Pitting	Pitting	Pitting	Pitting
Precipitation hardened alloy	1	IGC	IGC	—	—
	2	IGC	IGC	IGC	IGC
	3	IGC	IGC	Pitting	Pitting

Al alloys in Table 2 shows that the corrosion mode in all welding regions for Alloy 1 and 2, and BM and HAZ of Alloy 3 are controlled by intergranular corrosion, while the TMAZ and nugget zone of Alloy 3 is dominated by pitting corrosion. Thus, the Zn-containing Al-Mg alloy exhibits obvious intergranular corrosion which is greatly related to the environment near the grain boundary, such as the precipitation, intermetallics and/or precipitate free zones, and the Zn addition combined with aging treatment obviously cause the variation of the corrosion mode.

Table 3 shows the corrosion potentials (E_{corr}) and corrosion current densities (I_{corr}) for cathodic branches in the BM and nugget zone of all three alloys in the strain hardening temper. It can be found that both two values for the BM of Alloy 1 are much negative, and higher than those in the nugget zone, showing higher corrosion tendency and corrosion rates. For Alloy 2, a relatively lower corrosion tendency and corrosion rates in the BM is obtained, due mainly to its much lower I_{corr}. The E_{corr} and I_{corr} in the BM for Alloy 3 are much positive and lower than those in the nugget zone, showing lower corrosion tendency and corrosion rates. The differences of E_{corr} and I_{corr} between BM and nugget zone for Alloy 3 are much higher than Alloy 1 and 2, showing a severe micro-galvanic corrosion. Also, Table 3 shows E_{corr} and I_{corr} for cathodic branches in the BM and nugget zone of all three alloys in the precipitation hardening temper, and it indicates that E_{corr} and I_{corr} in the BM for the three alloys are much negative and higher than those in the nugget zone, corresponding to a higher corrosion tendency and corrosion rates in the BM region. The electro-chemical results presented here show the same corrosion tendency as those in Table 1.

Table 3 Corrosion potential and corrosion current density of BM and nugget zone of all three alloys

Alloy		E_{corr}/mV		I_{corr}/mA·cm^{-2}	
		BM	Nugget	BM	Nugget
Strain hardened alloy	1	–796.9	–749.5	7.9×10^{-7}	4.1×10^{-7}
	2	–785.9	–767.2	1.3×10^{-6}	4.2×10^{-6}
	3	–756.3	–802.5	7.1×10^{-7}	4.1×10^{-6}
Precipitation hardened alloy	1	–820.9	–747.1	9.0×10^{-7}	4.6×10^{-7}
	2	–901.1	–781.9	4.9×10^{-6}	1.7×10^{-6}
	3	–922.1	–807.6	6.6×10^{-6}	2.3×10^{-6}

The application of tensile stresses on the Al alloy can dramatically decrease the corrosion potential and thus increases the corrosion susceptibility of the alloy[19]. Residual stress also has an important effect on the intergranular corrosion behavior of the FSWed Al alloy. Previous researches showed that the residual stress in the TMAZ is higher than those in the WNZ, HAZ and BM [20-23]. As a result, for the strain hardened alloy, the corrosion depth in the TMAZ is higher than those in the WNZ, HAZ and BM. However, proper heat treatment can greatly decrease the residual stress in the FSWed joint[23]. It is assumed that the residual stress in the FSWed joint for the precipitation hardened alloy is quite lower than that of the strain hardened alloy. Thus, for the precipitation hardened alloy, the corrosion depth is controlled by the microstructure rather than the residual stress.

2.3 TEM characterization

Fig.5 shows the bright field TEM images in the BM and nugget zone for the strain hardened Alloy 1 and 3, and the statistical results of the number fraction and size of precipitates in the matrix and distribution of precipitates at the grain boundary for strain-hardened alloys are given in Table 4. For the Zn-free Al alloy, most precipitates are decorated along the grain boundary both in the BM and nugget zone while the number of the matrix precipitates is very low (Fig.5a~5d). The continuous/semi-continuous distribution of GBPs in the BM and nugget zone are almost similar, but the average grain size in the BM is quite larger than that in the nugget zone. It has been found that the corrosion can be easily occurred along an elongated grain rather than an equiaxed grain [24-26], and thus, the BM will possess higher corrosion depth than the nugget zone for the strain-hardened Zn-free Al alloy, which is in line with the results in Table 1. For the Zn-containing Al alloy, the GBPs (as marked by "A" in Fig.5h) in the nugget zone are mostly continuous or semi-continuous along the grain boundary with an average PFZ width of 114 nm (as marked by "B" in Fig.5h), as shown in Fig.5g, 5h, but no GBPs can be observed in the BM (Fig.5e). The intragranular precipitates are distributed homogeneously both in the BM and nugget zone while the average grain size in the BM is much larger than that in the nugget zone (Fig.3). The relatively poor corrosion resistance in the nugget zone is mainly due to the continuous distribution of GBPs and the formation of PFZ adjacent to the GBPs (The potential difference between the GBPs and PFZ may greatly contribute to the galvanic corrosion between them). The homogeneously distributed precipitates in the matrix result in the pitting corrosion in the strain-hardened Zn-containing Al alloy.

For the precipitation hardened Alloy 1 and 3, Table 5 presents the statistical results of the number fraction and size of precipitates in the matrix and distribution of precipitates at the grain boundary based on the TEM images in the BM and nugget zone (Fig. 6). The composition analysis in Fig.7 indicates that the GBPs are β-AlMg phase in the Zn-free Al alloy

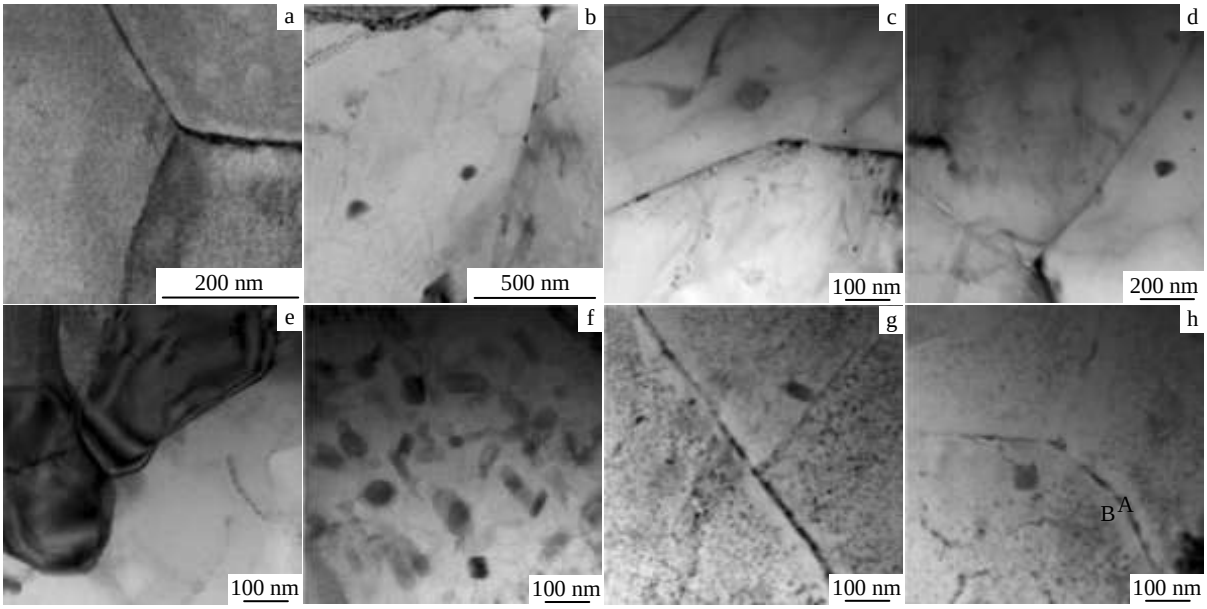

Fig.5 TEM images at grain boundaries of BM and nugget zone of the strain hardened Alloy 1 and Alloy 3: (a, b) Alloy 1 BM; (c, d) Alloy 1 nugget zone; (e, f) Alloy 3 BM; (g, h) Alloy 3 nugget zone

Table 4 Quantitative analysis of the number fraction (NF) and size of precipitates in the matrix and distribution of precipitates at the grain boundary for the strain hardened alloys

Alloy	Region	Ave. grain size/μm	GBPs distribution/%			Average PFZ width/nm	Matrix precipitates	
			Continuous	Semi-continuous	Clean		Average size/nm	NF/%
1	BM	15.8	75	12.5	12.5	—	—	—
	Nugget	3.1	72	14	14	—	—	—
3	BM	16.6	0	0	100	—	62.2	10
	Nugget	2.9	41	52	7	114	6.5	13.5

Table 5 Number fraction (NF) and size of precipitates in the matrix and distribution of precipitates at the grain boundary for the precipitation hardened Al alloys

Alloy	Region	Ave. grain size/μm	GBPs distribution/%			Average PFZ width/nm	Matrix precipitates	
			Continuous	Semi-continuous	Clean		Average size/nm	NF/%
1	BM	14.5	75	25	0	—	—	—
	Nugget	3.5	75	25	0	—	—	—
3	BM	13.3	100	0	0	357	23.85	16.9
	Nugget	3.8	0	93	7	183	9.6	13.5

and T-AlZnMgCu phase in the Zn-containing Al alloy. For the precipitation hardened Zn-free Al alloy, the microstructures both in the BM and nugget zone are almost same to those in the strain hardened Zn-free Al alloy: continuously or semi-continuously distributed GBPs and rarely appeared matrix precipitates. The relatively higher corrosion rate and corrosion depth in the BM are due mainly to its lager and elongated grains rather than smaller equiaxed grains in the nugget zone. For the precipitation hardened Zn-containing Al alloy, the GBPs in the BM are almost continuously distributed with an average PFZ width of 357 nm while the GBPs in the nugget zone are almost semi-continuously distributed with an average PFZ width of 183 nm. The average size of the intragranular precipitates in the BM is relatively larger than those in the nugget zone. The higher corrosion rate and depth in the BM is mainly because of the continuous GBPs distribution and the formation of relatively wider PFZ, while semi-continuously distributed GBPs and a higher number fraction of the intragranular precipitates result in pitting corrosion in the nugget zone. Thus, under the same T6 treatment, the corrosion (depth) of the BM and nugget zone cannot be concurrently optimized; however, other aging treatments, such as double-/three-step aging treatment or prolonging the aging times might be possible to gain good precipitation distribution in the BM and nugget zone.

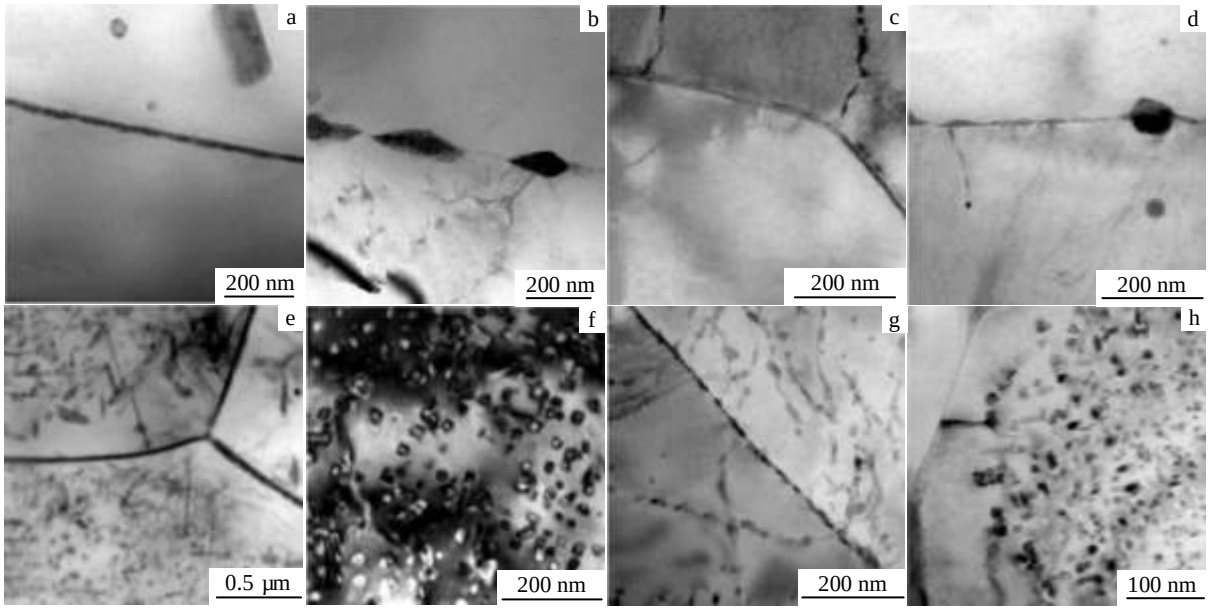

Fig. 6 TEM images at grain boundaries of BM and nugget zone of the precipitation hardened Alloy 1 and Alloy 3: (a, b) Alloy 1 BM; (c, d) Alloy 1 nugget zone; (e, f) Alloy 3 BM; (g, h) Alloy 3 nugget zone

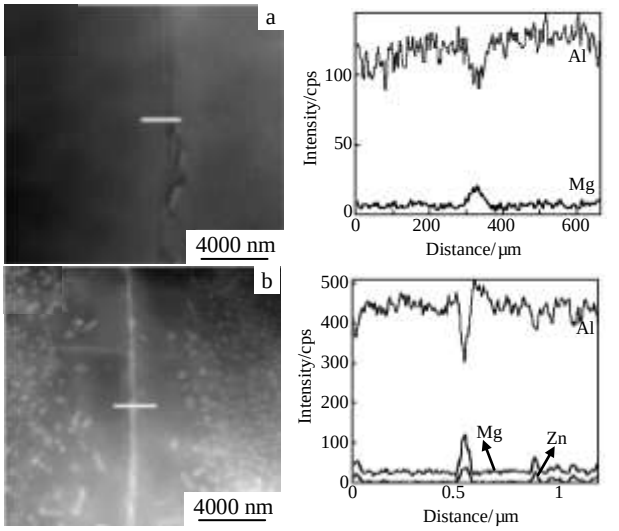

Fig.7 EDS composition analysis near the grain boundary of Alloy 1 (a) and 3 (b)

3 Conclusions

1) For the FSWed Zn-modified Al-Mg alloys the dominating corrosion mode is changed from intergranular to pitting corrosion, mainly because the intragranular precipitates in the Zn-modified Al alloy are easier to precipitate compared to the grain boundary precipitation in the Zn-free Al alloy. However, the precipitation hardened Al alloy shows a severe galvanic corrosion tendency compared to strain hardened Al alloy.

2) For traditional Al-Mg alloys, the corrosion is easier to take place at the BM and HAZ, but the smaller grain size in the nugget zone can dramatically decrease the corrosion rate compared to that of the BM and HAZ. For strain-hardened Zn-modified Al-Mg alloy, the corrosion is prone to take place at the nugget zone because of the continuous GBPs distribution and the formation of PFZ adjacent to the grain boundary, but the GBPs are discontinuously distributed at the BM with no PFZ formation. For the precipitation hardened Al alloys, the corrosion is easier to occur and propagate at the BM and HAZ for the relatively continuous GBPs distribution and wider PFZ in the BM compared to that in the nugget zone.

References

1 Mishra R S, Mahoney M W. *Friction Stir Welding and Processing*[C]. USA: ASM international, 2007: 51

2 Sato Y S, Kokawa H, Enomoto M *et al*. *Metallurgical and Materials Transactions A*[J], 1999, 30(9): 2429

3 Threadgill P L, Leonard A J, Shercliff H R *et al*. *International Materials Reviews*[J], 2009, 54: 49

4 Fonda R W, Pao P S, Jones H N *et al*. *Materials Science and Engineering A*[J], 2009, 519(1): 1

5 Hariri M B, Shiri S G, Yaghoubinezhad Y *et al*. *Materials & Design*[J], 2013, 50: 620

6 Lumsden J B, Mahoney M W, Rhodes C J *et al*. *Corrosion*[J], 2003, 59(3): 212

7 Wadeson D A, Zhou X, Thompson G E *et al*. *Corrosion Science*[J], 2006, 48(4): 887

8 Jariyaboon M, Davenport A J, Ambat R *et al*. *Corrosion Science*[J], 2007, 49(2): 877

9 Jariyaboon M, Davenport A J, Ambat R *et al*. *Anti-Corrosion*

Methods and Materials[J], 2010, 57(2): 83
10 Sato Y S, Kokawa H, Enomoto M *et al*. *Metallurgical and Materials Transactions A*[J], 1999, 30(12): 3125
11 Ipekoğlu G, Erim S, Çam G. *Metallurgical and Materials Transactions A*[J], 2014, 45(2): 864
12 Aydın H, Bayram A, Durgun İ. *Materials & Design*[J], 2010, 31(5): 2568
13 Proton V, Alexis J, Andrieu E *et al*. *Journal of the Electrochemical Society*[J], 2011, 158(5): C139
14 Paglia C S, Buchheit R G. *Materials Science and Engineering A*[J], 2008, 492(1): 250
15 Paglia C S, Jata K V, Buchheit R G. *Materials Science and Engineering A*[J], 2006, 424(1): 196
16 Proton V, Alexis J, Andrieu E *et al*. *Corrosion Science*[J], 2013, 73: 130
17 Meng C, Zhang D, Cui H *et al*. *Journal of Alloys and Compounds*[J], 2014, 617: 925
18 Cao C, Zhang D, He Z B *et al*. *Materials Science and Engineering: A*[J], 2016, 666: 34
19 Liu X, Frankel G S, Zoofan B *et al*. *Corrosion Science*[J], 2004, 46(2): 405
20 Fratini L, Pasta S, Reynolds A P. *International Journal of Fatigue*[J], 2009, 31(3): 495
21 Peel M, Steuwer A, Preuss M *et al*. *Acta Materialia*[J], 2003, 51(16): 4791
22 Feng Z, Wang X L, David S A *et al*. *Science and Technology of Welding & Joining*[J], 2007, 12(4): 348
23 Pouget G, Reynolds A P. *International Journal of Fatigue*[J], 2008, 30(3): 463
24 Lifka B W, Sprowls D O. *Corrosion*[J], 1966, 22(1): 7
25 Kelly D J, Robinson M J. *Corrosion*[J], 1993, 49(10): 787
26 Robinson M J, Jackson N C. *British Corrosion Journal*[J], 1999, 34(1): 45

搅拌摩擦焊接 Al-Mg-(Zn)合金的腐蚀行为

侯陇刚[1]，于佳佳[1]，张　迪[1]，庄林忠[1,2]，周　利[3]，张济山[1]

(1. 北京科技大学 新金属材料国家重点实验室，北京 100083)

(2. 塔塔钢铁，1970 CA 艾默伊登，荷兰)

(3. 哈尔滨工业大学（威海）山东省特种焊接技术重点实验室，山东 威海 264209)

摘　要：研究了搅拌摩擦焊接含 Zn Al-Mg 合金的腐蚀行为及焊后热处理对搅拌摩擦焊接合金腐蚀行为的影响。结果表明，经焊后热处理后不同焊接区的最大腐蚀深度和主导腐蚀模式随 Zn 含量增加而发生明显变化。Zn 的加入使主导腐蚀模式由晶间腐蚀变为点蚀。与加工硬化态合金相比，时效硬化态合金具有严重的电偶腐蚀倾向。对于析出强化 Al-Mg-Zn 合金而言，这在很大程度上与不连续分布的晶界析出相及丰富的晶内析出相的形成密切相关，而对无 Zn 的 Al-Mg 合金，则与连续分布的晶界 β-AlMg 相相关。

关键词：铝合金；搅拌摩擦焊接；晶间腐蚀；析出；组织

作者简介：侯陇刚，男，1982 年生，博士，助理研究员，北京科技大学新金属材料国家重点实验室，北京 100083，电话：010-82375844，E-mail: lghou@skl.ustb.edu.cn